A Data-Driven MPC Approach for Virtually Coupled Train Set with Non-Analytic Space-Time-Separation Distance

Abstract

The emerging virtual coupling technology aims to operate multiple train units in a virtually coupled train set (VCTS) at a minimal but safety distance. To guarantee collision avoidance, the safety distance should be calculated using the state-of-the-art space-time separation principle that separates the emergency braking (EB) trajectories of two successive units during the whole EB process. In this case, the minimal safety distance is usually numerically calculated without an analytic formulation. Thus, the constrained VCTS control problem is hard to be addressed with space-time separation, which is still a gap in the existing literature. To solve this problem, we propose a distributed economic model predictive control (DEMPC) approach with computation efficiency and theoretical guarantee. Specifically, to alleviate the computation burden, we transform implicit safety constraints into explicitly linear ones, such that the optimal control problem in DEMPC is a quadratic programming problem that can be solved efficiently. For theoretical analysis, sufficient conditions are derived to guarantee the recursive feasibility and stability of DEMPC, employing compatibility constraints, tube techniques and terminal ingredient tuning. Moreover, we extend our approach with globally optimal and distributed online EB configuration methods to further shorten the minimal distance among VCTS. Finally, experimental results demonstrate the performance and advantages of the proposed approaches.

Keywords: virtually coupled train set, space-time separation, non-analytic system, data-driven model predictive control

1. Introduction

Virtual coupling has drawn widely attention in recent years Wu et al. (2023); Felez and Vaquero-Serrano (2023); Xun et al. (2022), due to its advantages in improving efficiency and flexibility for train operations. This technology aims to form multiple train units as virtually coupled train set (VCTS) by communication and control techniques instead of physical couplers. However, successive units keeps a minimal such that a VCTS still can operate as a single train Quaglietta et al. (2020).

In the roadmap of virtual coupling, train motion control should be addressed first Aoun et al. (2023), which is critical for two fundamental functions: train-following control and collision avoidance. The former is a function of automatic train operation (ATO) systems, and operates VCTS with a desired train-following behavior. The latter is a function of automatic train protection (ATP) systems, and prevents successive from rear-end collision.

Recently, we have realized VCTS operations at 80 km/h in field tests Liu et al. (2023); Luo et al. (2024a, 2023). The space-time separation principle is employed to guarantee (safety integral level 4) collision avoidance for VCTS. Its main idea is shown in Figure , where two successive units are separated by a space at any time in the emergency braking (EB) process[1]. Thus, using this principle, collision avoidance of VCTS can be guaranteed if the following distance between two successive units is larger than the space-time-separation distance (STSD). Due to the feature of space-time separation, STSD is usually calculated by solving a constrained nonlinear programming problem (NLP) Chai et al. (2024); Zhao and Ioannou (2015); Wang et al. (2022). It is well-known that the analytic solution to constrained NLP is hard to obtain, which means STSD is calculated numerically without an analytic function w.r.t. the states of two successive units.

However, non-analytic STSD imposes significant challenges to the train-following control for VCTS. (1) constraint satisfaction; (2) generalization performance; (3) instability from non-convex; (4) computation efficiency;

[1] It is different from the traditional space separation principle that only separates units at where they stop

2. Problem Statement

2.1. Notations

2.2. Train Dynamics

We adopt a fourth-order model to capture the train dynamics as

$$\begin{cases} \dot{s}_i = v_i \\ \dot{v}_i = a_i \\ \dot{a}_i = \dfrac{f_i - a_i}{T} \\ \dot{f}_i = \psi_i \end{cases} \tag{1}$$

where s_i, v_i and a_i, respectively, denote the position, speed and controlled acceleration of unit i in a VCTS with $n+1$ units (where unit 0 is the leader), f_i is the controlled force per unit mass and ψ_i is its derivative, and T is the actuation lag. To additionally address the external forces, the feedback linearization techniques (Luo et al., 2024a; Bian et al., 2022) can be employed, such that this model can be maintained in the same manner.

The continuous dynamics (1) can be rewritten into a compact form $z_i = [s_i, v_i, a_i]^T$. Due to the discrete-time sampling of train states, we use $z_i(k) = [s_i(k), v_i(k), a_i(k)]^T$ to denote the sampled state at time instant k with a sampling interval τ.

2.3. Space-Time Separation and Calculation of Non-Analytic STSD

The main idea of space-time separation is to separate the EB trajectories of two successive train units at all time instants in the EB process. The main steps to calculate non-analytic STSD are given as follows. For more details, please see Chai et al. (2024); Wang et al. (2022).

We first model the EB dynamics of trains as

$$z_i^{EB}(t+1) = g_i^{EB}(z_i^{EB}(t), b_i) \tag{2}$$

where t and $z_i^{EB}(t) = [s_i^{EB}(t), v_i^{EB}(t), a_i^{EB}(t)]^T$, distinguishing from $z_i(k)$, denotes the time instant and calculated state in the EB process, respectively, and $g_i^{EB}(\cdot)$ is a nonlinear function to capture the EB dynamics, which involves some parameters, e.g. track gradients and curvatures, and the input arguments including train state z_i^{EB} and nominal EB rate b_i.

Then, the STSD $h_i(k)$, also as the safety distance between units $i-1$ and i, can be calculated by solving the following optimization problem:

$$h_i(k) = \min_{s_i^{EB}(0)} s_{i-1}^{EB}(0) - L - s_i^{EB}(0) \tag{3a}$$

s.t.

$$z_{i-1}^{EB}(0) = z_{i-1}(k), z_i^{EB}(0) = [s_i^{EB}(0), v_i(k), a_i(k)]^T \tag{3b}$$

$$z_i^{EB}(t+1) = g_i^{EB}(z_i^{EB}(t), b_i), \quad \forall t \in \mathbb{N}_0^{t_{EB}} \tag{3c}$$

$$s_{i-1}^{EB}(t) - L - s_i^{EB}(t) \geq s_m, \quad \forall t \in \mathbb{N}_0^{t_{EB}} \tag{3d}$$

where t_{EB} denotes the total length of the EB process and s_m is a safety margin. The constraint (3d) implies the ideal of space-time separation, as shown in Figure .

Due to the EB dynamics (3c) is nonlinear, we cannot get the exact analytic solution of this NLP problem. However, there are some useful numerical methods Wang et al. (2022); Zhao and Ioannou (2015); Chai et al. (2024) proposed to solve this problem. Thus, we can only get the exact value of STSD w.r.t. certain input arguments, which is calculated by a non-analytic function. However, it still guarantees collision avoidance, since the calculation model (3) is clearly defined.

2.4. VCTS Control

Based on the above formulation, we design a spacing policy $d_i(k)$ as

$$d_i(k) = h_i(k) + c_m \tag{4}$$

where c_m is a control margin accounting for tracking errors. Then, the equilibrium points for VCTS can be selected as

$$s_{i-1}(k) - L - s_i(k) - d_i(k) = 0, v_{i-1}(k) - v_i(k) = 0, a_{i-1}(k) - a_i(k) = 0, f_{i-1}(k) - f_i(k) = 0 \tag{5}$$

By defining the relative states as $\Delta s_i(k) = s_{i-1}(k) - L - s_i(k) - d_i(k)$, $\Delta v_i(k) = v_{i-1}(k) - v_i(k)$, $\Delta a_i(k) = a_{i-1}(k) - a_i(k)$ and $\Delta f_i(k) = f_{i-1}(k) - f_i(k)$, we can formulate the non-analytic system dynamics for all followers $i \in \mathbb{N}_1 n$ as

$$x_i(k+1) = f_i(x_i(k)) + Bu_i(k) \tag{6}$$

where the system state $x_i(k) = [\Delta s_i(k), \Delta v_i(k), \Delta a_i(k), \Delta f_i(k), v_i(k), a_i(k), f_i(k)]^T$, the control input $u_i(k) = [\psi_{i-1}(k), \psi_i(k)]^T$, $f_i(\cdot)$ is a non-analytic nonlinear function and B is a matrix. Note that the system state $x_i(k)$ includes both relative and absolute states, since the spacing policy $d_i(k)$ is nonlinear w.r.t. the absolute states of the two successive units $i-1$ and i. The formulation of this model is control-affine according to the continuous dynamics (1) and the definition of relative states (5), and the nonlinearity only exists in the order of $\Delta s_i(k)$.

For collision avoidance, each unit should satisfy a safety constraint

$$\Delta s_i(k) \geq -c_m \tag{7}$$

Besides, considering the limitation from tracks and trains, each unit should also satisfy a speed constraint

$$0 \leq v_i(k) \leq v_{max} \tag{8}$$

where v_{max} is the maximum speed. To avoid actuator saturation, each unit should satisfy a force constraint

$$f_{min} \leq f_i(k) \leq f_{max} \tag{9}$$

where f_{min} and f_{max} are the minimum and maximum controlled forces, respectively. Additionally, for passenger comfort, we further consider an input constraint

$$u_{min} \leq u_i(k) \leq u_{max} \tag{10}$$

where u_{min} and u_{max} are the minimum and maximum control input, respectively. For simplicity, we rewrite constraints (7)-(9) as $x_i(k) \in \mathbb{Z}$ and (10) as $u_i(k) \in \mathbb{U}$.

Thus, for the non-analytic system (6), the control objective is to stabilize a reference state $r = [0, 0, 0, 0, v_r, 0, 0]^T$ with a reference speed v_r[2], while satisfying constraints (7)-(9). However, it is not trivial to achieve this objective in MPC, since the system dynamics are non-analytic and nonlinear, which greatly influences computation efficiency, feasibility and stability. To this end, we propose a DMPC approach in the next section.

3. DMPC Designs

This section designs the DMPC approach. First, we formulate a data-driven prediction model without the knowledge of non-analytic system (6). Then, the DMPC framework is proposed. Next, we analyze the theoretical performance of DMPC. Finally, a dual-mode online implementation algorithm is presented.

[2]We suppose the leader exactly tracks the reference speed.

3.1. Data-Driven Prediction Models

3.1.1. Data-Driven Trajectory Prediction

Due to the non-analytic formulation of system (6), we deploy a data-driven model to predict the future trajectory of state x_i.

Based on behavioral system theory, data-driven modeling methods are usually applied to linear systems rather than nonlinear systems. Thus, we first consider that, linearized from system (6), there exists a linear model

$$x_i(k+1) = \tilde{A}x_i(k) + Bu_i(k) + \tilde{e}_i \tag{11}$$

where $\tilde{A}$ is a state-transfer matrix and $\tilde{e}_i$ is a linearized error which follows

$$\tilde{e}_i = f_i(x_i(k)) - \tilde{A}x_i(k) \tag{12}$$

Then, we introduce the Hankel matrix $H_\ell(x)$ defined by

$$H_\ell(x) = \begin{bmatrix} x(0) & x(1) & \dots & x(M-\ell) \\ x(1) & x(2) & \dots & x(M-\ell+1) \\ \vdots & \vdots & \ddots & \vdots \\ x(\ell-1) & x(\ell) & \dots & x(M-1) \end{bmatrix} \tag{13}$$

with M states $x([0:M-1])$ and an horizon ℓ. Then, the results in the following lemma show that linearized system (11) can be captured by linear equations using the Hankel matrix, which draws the inspiration from Berberich et al. (2022b).

Lemma 1. *Suppose there exist measured output data $x_i^d([0:M-1])$ and input data $u_i^d([0:M-1])$ where $u_i^d([0:M-1])$ is PE such that*

$$\operatorname{rank}\left(\begin{bmatrix} H_\ell(u_i^d) \\ x_i([0:M-\ell])^T \\ \mathbb{I}_{M-\ell+1}^T \end{bmatrix}\right) = 2\ell + 7 + 1 \tag{14}$$

Then, $\hat{x}_i([0:\ell-1])$ and $\hat{u}_i([0:\ell-1])$ are output and input trajectories of system (11), if and only if there exists a vector α such that

$$\begin{bmatrix} \hat{u}_i([0:\ell-1]) \\ \hat{x}_i([0:\ell-1]) \end{bmatrix} = \begin{bmatrix} H_\ell(u_i^d) \\ H_\ell(x_i^d) \end{bmatrix} \alpha, \quad \sum_{j=0}^{M-\ell} [\alpha]_j = 1 \tag{15}$$

Proof. We first consider a linearized model holding

$$x_i^d([j:j+\ell-1]) = \Gamma_A x_i^d(j) + \Gamma_B u_i^d([j:j+\ell-1]) + \Gamma_D \tilde{e} \tag{16}$$

where Γ_A, Γ_B and Γ_D are matrices depending on $\tilde{A}$, B and $\tilde{e}$. Then, from the equation (15), it follows

$$\begin{aligned} \hat{x}_i([0:\ell-1]) &= \textstyle\sum_{j=0}^{M-\ell} x_i^d([j:j+\ell-1])[\alpha]_j \\ &= \textstyle\sum_{j=0}^{M-\ell} \left(\Gamma_A x_i^d(j) + \Gamma_B u_i^d([j:j+\ell-1]) + \Gamma_D \tilde{e}\right)[\alpha]_j \\ &= \Gamma_A \hat{x}_i(0) + \Gamma_B \hat{u}_i([0:\ell-1]) + \Gamma_D \tilde{e} \end{aligned} \tag{17}$$

where the last equality holds due to $\sum_{j=0}^{M-\ell}[\alpha]_j = 1$. This implies $\hat{x}_i([0:\ell-1])$ and $\hat{u}_i([0:\ell-1])$ are output and input trajectories of (11) if the equation (15) holds.

Next, to prove "only if", let $x_i([0:\ell-1])$ and $u_i([0:\ell-1])$ be the output and input trajectories of (11), such that it follows

$$\begin{aligned} \hat{x}_i([0:\ell-1]) &= \Gamma_A \hat{x}_i(0) + \Gamma_B \hat{u}_i([0:\ell-1]) + \Gamma_D \tilde{e} \\ &= \textstyle\sum_{j=0}^{M-\ell} \left(\Gamma_A x_i^d(j) + \Gamma_B u_i^d([j:j+\ell-1]) + \Gamma_D \tilde{e}\right)[\alpha]_j \\ &= \textstyle\sum_{j=0}^{M-\ell} x_i^d([j:j+\ell-1])[\alpha]_j \\ &= H_\ell(x_i^d)\alpha \end{aligned} \tag{18}$$

where the second equality follows from that the condition (14) holds, such that

$$\begin{bmatrix} H_\ell(u_i^d) \\ x_i^d([0:M-\ell])^T \\ \mathbb{I}_{M-\ell+1}^T \end{bmatrix} \alpha = \begin{bmatrix} \hat{u}_i([0:M-\ell]) \\ \hat{x}_i(0) \\ 1 \end{bmatrix} \tag{19}$$

and the third equality follows from (16). This implies the condition (15) holds if $x_i([0:\ell-1])$ and $u_i([0:\ell-1])$ be the output and input trajectories of (11), which completes the proof. □

3.1.2. Boundedness of Linearization Error

The results in Lemma 1 imply that we could find a linearized model to capture the dynamics of system (6). However, that model is linearized based on the measured data, which means the linear model just matches the specified data trajectory rather than arbitrary real-time trajectories. Thus, there inevitably exist linearization errors when predicting the future trajectory.

To facilitate constraint satisfaction and stability for DMPC, we analyze the boundedness of linearization errors in the following proposition.

Proposition 1. *Consider a predicted trajectory $\hat{x}_i([0:\ell-1])$ of dynamics (16) and an actual trajectory $x_i([0:\ell-1])$ of dynamics (6) resulted from the same inputs $\hat{u}_i([-1:\ell-2])$. Then, there exists constants $L_{i,x}, \bar{\xi}_i > 0$, such that the errors between them are bounded by*

$$\|x_i(j) - \hat{x}_i(j)\| \le \delta\hat{x}(j), \quad \forall j \in \mathbb{N}_0^{N-1} \tag{20a}$$

$$\delta\hat{x}(j+1) = L_{i,x}\delta\hat{x}(j) + \bar{\xi}_i, \quad \forall j \in \mathbb{N}_0^{N-1} \tag{20b}$$

with $\delta\hat{x}(0) = \bar{\xi}_i$.

Proof. From the linearized dynamics (11), we have

$$x_i(j+1) - \hat{x}_i(j+1) = f_i(x_i(j)) - \tilde{f}_i(\hat{x}_i(j)) \tag{21}$$

where $\tilde{f}_i$ denotes the linearized dynamics according to a state $\tilde{x}_i^d$ in the data trajectory, which follows $\tilde{f}_i(\tilde{x}_i^d) = f_i(\tilde{x}_i^d)$. Then, we have

$$\|f_i(x_i) - \tilde{f}_i(x_i)\| \le C_{i,x}\|x_i - x_i^d\|^2 \tag{22}$$

where constant $C_{i,x} > 0$. It follows from the Taylor's expansion and $x_i, \tilde{x}_i \in \mathbb{Z}$. Then, we can derive the bound of errors as

$$\begin{aligned} \|x_i(j+1) - \hat{x}_i(j+1)\| &= \|f_i(x_i(j)) - \tilde{f}_i(x_i(j))\| + \|\tilde{f}_i(x_i(j)) - \tilde{f}_i(\hat{x}_i(j))\| \\ &\le C_{i,x}\|x_i(j) - x_i^d(j)\|^2 + L_{i,x}\|x_i(j) - \hat{x}_i(j)\| \\ &\le L_{i,x}\|x_i(j) - \hat{x}_i(j)\| + \bar{\xi}_i \end{aligned} \tag{23}$$

where the first inequality holds if we select $L_{i,x}$ as the Lipschitz constant of $f_i(x_i, u_i)$ and $\bar{\xi}_i = \max_{x_i, x_i^d \in \mathbb{Z}} C_{i,x}\|x_i - x_i^d\|^2$. □

3.2. DMPC Scheme

Then, based on the above data-driven prediction model, we design the DMPC scheme in this part. The controller of DMPC is yielded by solving the following OCP:

$$\min_{\hat{x}_i(\cdot|k), \hat{u}_i(\cdot|k), \alpha_i(k)} J_i(k) = \sum_{j=0}^{N-1} \|\hat{x}_i(j|k) - r\|_Q^2 + \|\hat{u}_i(j|k)\|_R^2 + \|\alpha_i(k) - \alpha^r\|_{\lambda_\alpha}^2 \tag{24a}$$

s.t.

$$\begin{bmatrix} \hat{u}_i([-D:-1]|k) \\ \hat{x}_i([-D:-1]|k) \end{bmatrix} = \begin{bmatrix} u_i([k-D:k-1]) \\ x_i([k-D:k-1]) \end{bmatrix} \tag{24b}$$

$$\begin{bmatrix} \hat{u}_i([-D:N-1]|k) \\ \hat{x}_i([-D:N-1]|k) \\ 1 \end{bmatrix} = \begin{bmatrix} H_{D+N}(u_i^d) \\ H_{D+N}(x_i^d) \\ \mathbb{I}^T_{M-D-N+1} \end{bmatrix} \alpha_i(k) \tag{24c}$$

$$[\hat{u}_i(j|k)]_1 = [\hat{u}^*_{i-1}(j+1|k-1)]_2, \quad \forall j \in \mathbb{N}_0^N - 1 \tag{24d}$$

$$\hat{x}_i(j|k) \in \mathbb{Z} \ominus \mathbb{S}_i(j), \quad \forall j \in \mathbb{N}_0^N - 1 \tag{24e}$$

$$\hat{u}_i(j|k) \in \mathbb{U}, \quad \forall j \in \mathbb{N}_0^N - 1 \tag{24f}$$

$$[\hat{u}_i(j|k)]_2 - [\hat{u}^*_i(j+1|k-1)]_2 \in \tilde{\mathbb{U}}, \quad \forall j \in \mathbb{N}_0^N - 1 \tag{24g}$$

where $(j|k)$ denotes the future instant $k+j$, N is the prediction horizon, D is the length of past data to be used, $\alpha_i(k)$ is a vector for data-driven modeling and α^r is its linearized value at the reference state, Q, R and λ_α are weighting coefficients, $\mathbb{S}_i(j)$ and $\tilde{\mathbb{U}}$ are sets for constraint tightening and compatibility constraints, respectively, which will be introduced later. We use $\hat{x}^*_i(\cdot|k)$, $\hat{u}^*_i(\cdot|k)$ and $\alpha^*_i(k)$ to denote the optimizer of OCP (24), while appending $[\hat{u}^*_{i-1}(N|k-1)]_2 = [\hat{u}^*_{i-1}(N-1|k-1)]_2$.

Note that the proposed DMPC framework does not involve the non-analytic nonlinear system dynamics (6). Alternatively, we deploy the data-driven prediction model (24c), while (24b) substitutes the traditional initial condition $x_i(0|k) = x_i(k)$. Thus, OCP (24) is a standard QP problem that can be solved trivially and efficiently.

Specifically, α^r is calculated by solving the following OCP:

$$\alpha^r = \arg\min_{\alpha} \|\alpha\|^2_{\lambda_\alpha} \tag{25a}$$

s.t.

$$\begin{bmatrix} \mathbb{I}_{D+N} \otimes [0,0]^T \\ \mathbb{I}_{D+N} \otimes r \\ 1 \end{bmatrix} = \begin{bmatrix} H_{D+N}(u_i^d) \\ H_{D+N}(x_i^d) \\ \mathbb{I}^T_{M-D-N+1} \end{bmatrix} \alpha \tag{25b}$$

which yields a steady linear dynamics of system (6) at the reference state r. This design helps the data-driven prediction model (24c) fit the steady one, with the system state approaching the reference state.

Algorithm 1: Distributed implementation of DMPC

Offline preparation:
Prepare a database including x_i^d and u_i^d for each unit $i \in \mathbb{N}_0^{n-1}$, which satisfies the PE condition (14); Calculate α_i^r by solving (25);
Online computation:
Initialize $x_i([-D:-1])$, $u_i([-D:-1])$ and $\hat{u}^*_i([0:N-1]|-1)$ for all $i \in \mathbb{N}_0^n$ at instant $k=0$;
for $k = 0, 1, \ldots$ **do**
  for *all units* $i \in \mathbb{N}_1^n$ *in paralle* **do**
    Receive $\hat{u}^*_{i-1}([0:N-1]|k-1)$ from the preceding unit $i-1$;
    Solve OCP (24) and obtain $\hat{u}^*_i([0:N-1]|k)$;
    Send $\bar{u}^*_i([0:N-1]|k)$ to the following unit $i+1$ (if existed);
    Apply $u_i(k) = u^*_i(0|k)$;
  end
end

3.3. Theoretical Analysis

This part analyzes the constraint satisfaction and stability for DMPC. It is not trivial to guarantee the theoretical performance of DMPC, especially for distributed nonlinear systems. The existing work Berberich et al. (2021, 2022b) mainly focuses on centralized systems, and generally sets a terminal equality constraint, which imposes the terminal state reach the reference state. However, it requires an enough long prediction horizon, such that the terminal state can

be steered from the initial state to the reference state. Apparently, this method significantly increases the computation time of DMPC.

Alternatively, another work Bongard et al. (2023) cancels terminal equality constraints and investigates the local stability with a certain prediction horizon. The main idea is to find an attraction region corresponding to the prediction horizon, such that there exists a feedback controller to stabilize the system within the attraction region.

Enlightened by the above work, we will analyze the theoretical performance in the premise of some useful and practical assumptions.

3.3.1. Constraint Satisfaction

We first focus on the constraint satisfaction, i.e., feasibility, of DMPC (24). It is influenced by linearization errors and the mismatch between the actual and received information from the preceding unit. Thus, we deploy compatibility constraints and tighten the constraints in DMPC, such that the constraint satisfaction can be established in the following theorem.

Theorem 1. *If there exists a constant $L_u > 0$ and a set $\tilde{\mathbb{U}} = \{u : -\bar{u} \le u \le \bar{u}\}$ with a constant $\bar{u} > 0$, such that for all $j \in \mathbb{N}_0^{N-1}$ the tightened set $\mathbb{Z} \ominus \mathbb{S}_i(j)$ is not empty with $\mathbb{S}_i(-1) = \emptyset$ and holding*

$$\|x_i^+\| \le L_{i,x}\|x_i\| + \bar{\xi}_i + L_u\|[j\bar{u}, 0]^T\|, \forall x_i \in \mathbb{S}_i(j), x_i^+ \in \mathbb{S}_i(j+1) \tag{26}$$

then, $x_i(k+j) \in \mathbb{Z}$ for all $j \in \mathbb{N}_0^{N-1}$ and $x_i(k+j+1) = f_i(x_i(k+j)) + B[[u_{i-1}^*(0|k+j)]_2, [u_i^*(j|k)]_2]^T$.

Proof. For all $j \in \mathbb{N}_{-1}^{N-2}$, we have

$$\begin{aligned}
& \|x_i(k+j+1) - \hat{x}_i(j+1|k)\| \\
= \; & \|f_i(x_i(k+j)) + Bu_i(k+j) - \tilde{f}_i(\hat{x}_i(j|k)) - B\hat{u}_i(j|k)\| \\
= \; & \|f_i(x_i(k+j)) + B(\hat{u}_i(j|k) + u_i(k+j) - \hat{u}_i(j|k)) - \tilde{f}_i(\hat{x}_i(j|k)) - B\hat{u}_i(j|k)\| \\
\le \; & \|f_i(x_i(k+j)) - \tilde{f}_i(\hat{x}_i(j|k))\| + \|B(u_i(k+j) - \hat{u}_i(j|k))\| \\
\le \; & L_{i,x}\|x_i(k+j) - \hat{x}_i(j|k)\| + \bar{\xi}_i + L_u\|[j\bar{u}, 0]^T\|
\end{aligned} \tag{27}$$

where the last inequality follows from the results in Proposition 1 and L_u is selected from matrix B. Then, if the condition (26) holds, we have

$$x_i(k+j) \in \hat{x}_i(j|k) \oplus \mathbb{S}_i(j) \subseteq \mathbb{Z}, \quad j \in \mathbb{N}_0^{N-1} \tag{28}$$

which completes the proof. □

The results in Theorem 1 implies that the optimal control action $u_i^*(\cdot|k)$ can robustly guarantee constraint satisfaction in the next N steps. Thus, we conjecture that the DMPC is recursively feasible if the prediction horizon is sufficient long. However, the mathematical proof needs rigorous analysis of the dynamics out of the prediction horizon, which is difficult due to the non-analytic formulation of system (6). It will be interesting work in the future.

3.3.2. Stability

To analyze the stability of DMPC (24), we first consider a standard NMPC with OCP:

$$\min_{\hat{x}_i(\cdot|k), \hat{u}_i(\cdot|k)} J_i'(k) = \sum_{j=0}^{N-1} \|\hat{x}_i(j|k) - r\|_Q^2 + \|\hat{u}_i(j|k)\|_R^2 \tag{29a}$$

s.t. constraints (24d)-(24g) and

$$\hat{x}_i(0|k) = x_i(k) \tag{29b}$$

$$\hat{x}_i(j+1|k) = f_i(\hat{x}_i(j|k), \hat{u}_i(j|k)) \tag{29c}$$

which are same to DMPC (24) besides substituting the initial condition (24b) and prediction model (24c) by (29b) and (29c), respectively. Then, we make the following assumptions concerning the optimizer of OCP (24) and (29).

Assumption 1. *There exists constants $c_x, \bar{V}' > 0$ and a Lyapunov function $V_i'(k) = J_i'^*(k)$ which satisfies $V_i'(k+1) - V_i'(k) \le -c_x\|x_i(k)\|^2$ for all $V_i'(k) \le \bar{V}'$.*

This assumption establishes a local asymptotic stability for NMPC (29), which can be satisfied with the knowledge of bounds of $\partial f_i(x_i)/\partial x_i$ Berberich et al. (2022a); Kohler and Allgower (2019); Luo et al. (2024b).

Assumption 2. *Use $\hat{u}_i^*(\cdot|k)$ and $\tilde{u}_i^*(\cdot|k)$ to denote the optimizer of DMPC (24) and NMPC (29), respectively. Then, the difference between them is upper bounded by*

$$\|\hat{u}_i^*(j|k) - \tilde{u}_i^*(j|k)\| \leq \epsilon_u(j), \quad \forall j \in \mathbb{N}_0^{N-1} \tag{30}$$

Similar utilization can be found in Berberich et al. (2022b) and Bongard et al. (2023) with mathematical proof. Despite our DMPC formulation is slight different from the ones in their work, we still can observe an upper bound ϵ_u from experimental results to satisfy this assumption. Then, it facilitates the analysis of optimal trajectories yielded by (24).

Proposition 2. *Use $\hat{x}_i^*(\cdot|k)$ and $\tilde{x}_i^*(\cdot|k)$ to denote the optimal states of DMPC (24) and NMPC (29), respectively. Then, if Assumption 2 holds, the difference between them is upper bounded by*

$$\|\hat{x}_i^*(j|k) - \tilde{x}_i^*(j|k)\| \leq \epsilon_{i,x}(j), \quad \forall j \in \mathbb{N}_0^{N-1} \tag{31}$$

where $\epsilon_{i,x}(j+1) = L_{i,x}\epsilon_{i,x}(j) + \bar{\xi}_i + L_u\epsilon_u(j)$ and $\epsilon_{i,x}(0) = \max_{x\in\mathbb{S}_i(0)} \|x\|$.

Proof. Using the similar steps aforementioned, we have

$$\begin{aligned} & \|\hat{x}_i^*(j+1|k) - \tilde{x}_i^*(j+1|k)\| \\ = \; & \|\tilde{f}_i(\hat{x}_i^*(j|k)) + B\hat{u}_i^*(j|k) - f_i(\tilde{x}_i^*(j|k)) + B\tilde{u}_i^*(j|k)\| \\ = \; & \|\tilde{f}_i(\hat{x}_i^*(j|k)) - f_i(\tilde{x}_i^*(j|k))\| + \|B(\hat{u}_i^*(j|k) - \tilde{u}_i^*(j|k))\| \\ \leq \; & L_{i,x}\|\hat{x}_i^*(j|k) - \tilde{x}_i^*(j|k)\| + \bar{\xi}_i + L_u\epsilon_u(j) \end{aligned} \tag{32}$$

Thus, we can induct that $\|\hat{x}_i^*(j|k) - \tilde{x}_i^*(j|k)\| \leq \epsilon_{i,x}(j)$ holds for all $j \in \mathbb{N}_0^{N-1}$. □

Based on the above assumptions and proposition, we can finally establish stability for DMPC.

Theorem 2. *Suppose Assumptions 1 and 2 are satisfied. Then, there exists a constant $\varepsilon_x > 0$, such that the region $\mathbb{V} = \{x : \|x - r\| \leq \varepsilon_x\}$ is practically asymptotically stable for the system (6) with DMPC (24).*

Proof. Based on Assumption 2 and Proposition 2, we have (31). Then, select a Lyapunov function $V_i(k) = \sum_{j=0}^{N-1} \|\hat{x}_i^*(j|k) - r\|_Q^2 + \|\hat{u}_i^*(j|k)\|_R^2$, such that it follows

$$\begin{aligned} & V_i(k+1) - V_i(k) \\ = \; & \textstyle\sum_{j=0}^{N-1} \|\hat{x}_i^*(j|k+1) - r\|_Q^2 + \|\hat{u}_i^*(j|k+1)\|_R^2 - \left(\sum_{j=0}^{N-1} \|\hat{x}_i^*(j|k) - r\|_Q^2 + \|\hat{u}_i^*(j|k)\|_R^2\right) \\ \leq \; & \textstyle\sum_{j=0}^{N-1} \|\tilde{x}_i^*(j|k+1) - r\|_Q^2 + \|\epsilon_x(j)\|_Q^2 + 2\|\epsilon_x(j)\|_Q\|\tilde{x}_i^*(j|k+1) - r\|_Q + \|\tilde{u}_i^*(j|k+1)\|_R^2 + \|\epsilon_u\|_R^2 + 2\|\epsilon_u\|_R\|\tilde{u}_i^*(j|k+1)\|_R \\ & - \left(\textstyle\sum_{j=0}^{N-1} \|\tilde{x}_i^*(j|k) - r\|_Q^2 + \|\epsilon_x(j)\|_Q^2 - 2\|\epsilon_x(j)\|_Q\|\tilde{x}_i^*(j|k) - r\|_Q + \|\tilde{u}_i^*(j|k)\|_R^2 + \|\epsilon_u\|_R^2 - 2\|\epsilon_u\|_R\|\tilde{u}_i^*(j|k)\|_R\right) \\ \leq \; & -c_x\|x_i(k)\| + 2\textstyle\sum_{j=0}^{N-1} \|\epsilon_x(j)\|_Q(\|\tilde{x}_i^*(j|k+1) - r\|_Q + \|\tilde{x}_i^*(j|k) - r\|_Q) + \|\epsilon_u\|_R(\|\tilde{u}_i^*(j|k+1)\|_R + \|\tilde{u}_i^*(j|k)\|_R) \\ \leq \; & -c_x\|x_i(k)\| + c_\delta \end{aligned} \tag{33}$$

where the second inequality follows from Assumption 1 and $c_\delta = \max_{\tilde{x}_i(j)\in\mathbb{Z}_i\ominus\mathbb{S}_i(j),\tilde{u}_i\in\mathbb{U}} 4\sum_{j=0}^{N-1} \|\epsilon_x(j)\|_Q\|\tilde{x}_i(j) - r\|_Q + \|\epsilon_u\|_R\|\tilde{u}_i\|_R$. Thus, we can find an appropriate $\varepsilon_x > 0$, such that the region $\mathbb{V} = \{x : \|x - r\| \leq \varepsilon_x\}$ is practically asymptotically stable for the system (6). □

The above results demonstrate that the states of VCTS can be maintained in a region around the reference state by DMPC (24), rather than exactly converging to the reference state (i.e., asymptotic stability). It is resulted from the linearization errors in data-driven modeling. However, with approaching the reference state, linearization errors will keep decreasing, such that the states of VCTS will finally converge to a very small region around the reference state.

Despite that mathematical methods are not provided to tune the parameters of DMPC, we can summarize some empirical methods as follows. The value of Q and R can refer to the standard MPC tuning or feedback controller tuning, and the value of λ_α is directly proportional to the nonlinearity of systems.

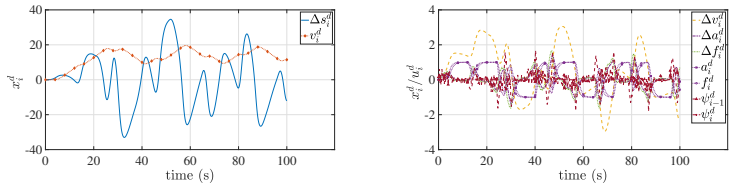

(a) (b)

Figure 1: Data trajectories used in experiments: (a) Δs_i^d and v_i^d; (b) The rest entries in x_i^d, and u_i^d.

4. Experimental Results

We adopt the calculation model of STSD in our previous field tests Liu et al. (2023); Luo et al. (2024a, 2023), which has been realized VCTS operation (for tests rather than daily operations) in Beijing Metro Line 11. The details of this model can be found in Wang et al. (2022).

4.1. Performance of DMPC

4.1.1. Data Trajectory

We first show the data trajectories x_i^d and u_i^d in Figures 1(a) and 1(b). The Hankel matrices made of x_i^d and u_i^d satisfy the PE condition (14) with the rank of $31 > 20 + 7 + 1$.

Through our experiments, we find that it is better to let data trajectories cover all pairs of states and inputs that will appear in the VCTS operation, such that the nonlinearity of VCTS dynamics (6) can be captured more accurately.

4.1.2. Cruising Case

We suppose that in this cruising case all units initially drives at the reference speed $v_r = 15$ km/h, and the following distance of each follower is initially larger than the spacing policy.

The speed trajectories are shown in Figures 2(a) and 2(b), where all followers first accelerate to shorten the following distance and finally keep driving at the reference speed. From Figure 2(c), we can find that the following distance between each two successive units converge to the spacing policy. Figure 2(d) demonstrates that the safety constraint (7) is satisfied. Moreover, the satisfaction of force constraint (9) and input constraint (10) are demonstrated by Figures 2(e) and 2(f).

In the above results, VCTS spends long time to converge to the reference state, which is caused by the low gain of controllers (i.e., small value of weighting coefficients and feedback gains). Through our experiments, we found that, due to the complex nonlinearity of system (6), controllers with higher gain are prone to oscillation around the reference state. During train operations, the oscillation of speed (or inputs) should be avoided to prevent from passenger discomfort or energy waste. Thus, despite that a higher gain could result in faster convergence, we tune the controllers with low gains.

4.1.3. Speed-Varying Case

We suppose that in this cruising case all units initially drives at the reference state r with a reference speed $v_r = 15$ km/h, and the reference speed will first increase and then reduce to the reference speed $v_r = 15$ km/h.

From Figures 3(a) and 3(b), we can find that the speed of each follower changes with its preceding unit. The relative speed is not equal to zero during the speed-varying phase, since the following distance should increase or decrease with the spacing policy. However, once the reference speed is fixed again, VCTS can finally converge to the reference state as well as the results in the cruising case. Moreover, Figure 3(c) demonstrates that the following distance can maintain around the spacing policy. The satisfaction of constraints (7)-(10) is shown in Figures 3(d)-3(f).

4.2. Advantages of DMPC

In this part, we compare the performance of DMPC and other approaches that potentially could address VCTS control with non-analytic STSD. Through the experimental results, we will emphasize the advantages of our approach.

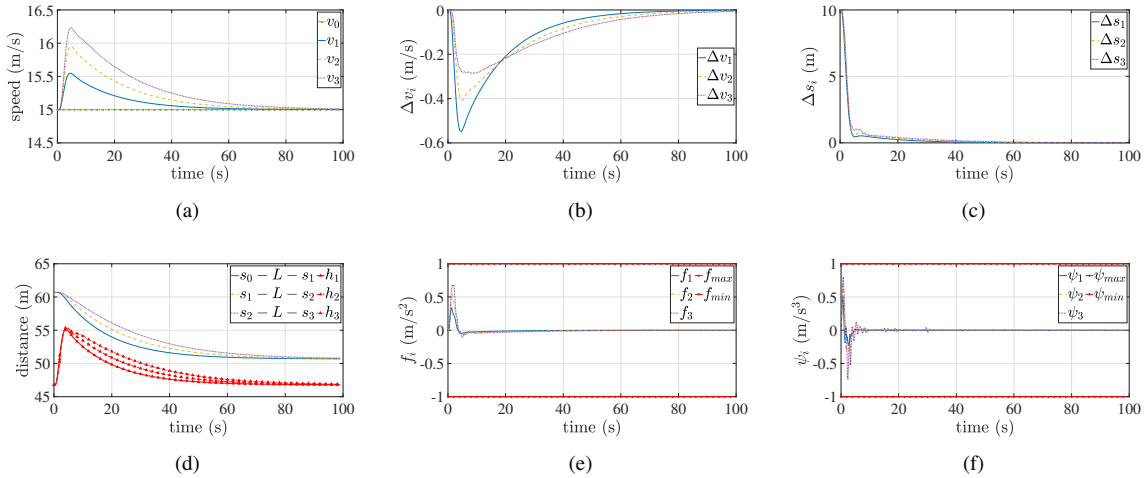

Figure 2: VCTS operation in the cruising case: (a)-(c) stability of speed v_i, relative speed Δv_i and the error of following distance Δs_i, respectively; (d)-(e) satisfaction of safety constraints (following distance $s_{i-1} - L - s_i$ and safety distance h_i), force constraints (controlled forces per unit mass f_i) and input constraints (control input $u_i = [\psi_{i-1}, \psi_i]^T$).

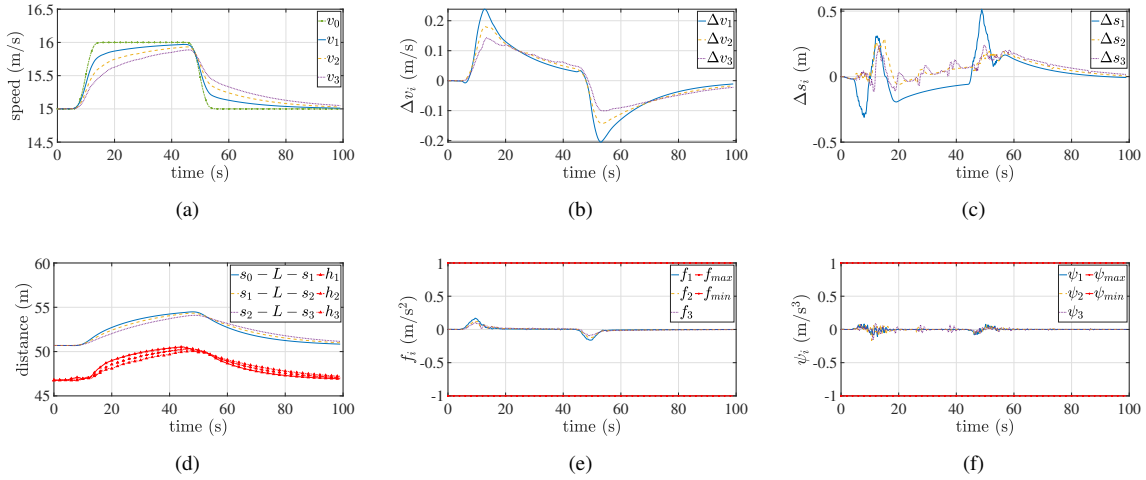

Figure 3: VCTS operation in the speed-varying case: (a)-(c) stability of speed v_i, relative speed Δv_i and the error of following distance Δs_i, respectively; (d)-(e) satisfaction of safety constraints (following distance $s_{i-1} - L - s_i$ and safety distance h_i), force constraints (controlled forces per unit mass f_i) and input constraints (control input $u_i = [\psi_{i-1}, \psi_i]^T$).

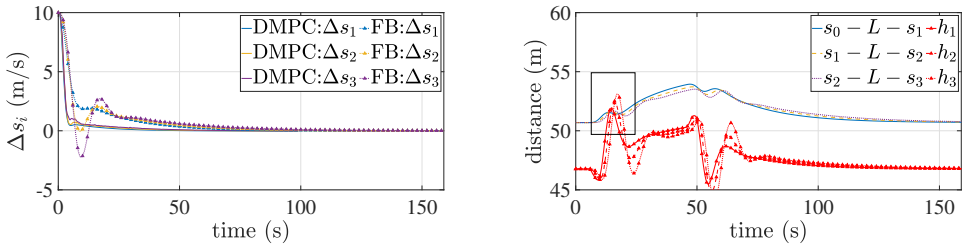

(a) (b)

Figure 4: Comparison of DMPC and feedback control: (a) chattering ('FB' denotes feedback control); (b) constraint violation (in the black rectangle) resulted from feedback control.

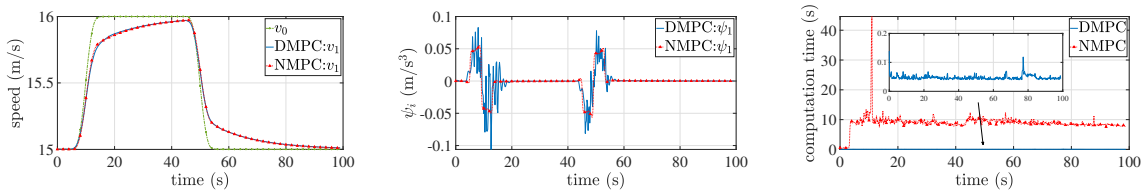

(a) (b) (c)

Figure 5: Comparison of DMPC and NMPC: (a) similar tracking performances; (b) bounded difference between control inputs; (c) computation efficiency.

4.2.1. Constraint Satisfaction: Compared with Feedback Control

Since system (6) is high-order and non-analytic, some feedback control methods based on analytic tuning, e.g., back-stepping, adaptive control and invariant control, are hard to exploit. Alternatively, to compare the general features of DMPC and feedback control, we deploy a standard proportional-integral-derivative controller $\psi_i(k) = Kx_i(k)$ with $K = [0.01, 0.1, 0.15, 0.6, 0, 0, 0]^T$ that is useful to address practically complex system like (6).

From Figure 4(a), we can find that feedback controller will result in chattering, when pursing similar responding as DMPC. Moreover, Figure 4(b) demonstrates that feedback control will easily violate constraints.

4.2.2. Computation Efficiency: Compared with Nonlinear MPC

To overcome the limitation of feedback control, we further employ a nonlinear MPC (NMPC) approaches and compare the performance with our approach. The formulation of NMPC is the same as (29), where the non-analytic system dynamics (6) are directly involved.

From Figure 5(a), we can find that the tracking performances of DMPC and NMPC are similar. We also illustrate the difference between control inputs of NMPC and DMPC in Figure 5(b). We can find that the differences are slight, which supports Assumption 2.

However, the computation time of DMPC is much less than NMPC, because the latter one solves the optimization problem (3) in each iteration solving OCP (29). As shown in 5(c), NMPC costs over 10 s to calculate a controller, while DMPC only costs less than the sampling interval. Specifically, DMPC saves more than 99.53% computation time than NMPC. Moreover, another critical problem of NMPC is that it potentially yields local-optimal controllers from the non-convex OCP. This problem could make VCTS operation unstable.

4.2.3. Smoothness and Modeling Accuracy: Compared with Adaptive MPC

To alleviate the computation burden of MPC, we formulate an adaptive MPC (AMPC) approach whose prediction model is linear and adaptively updated using online system identification.

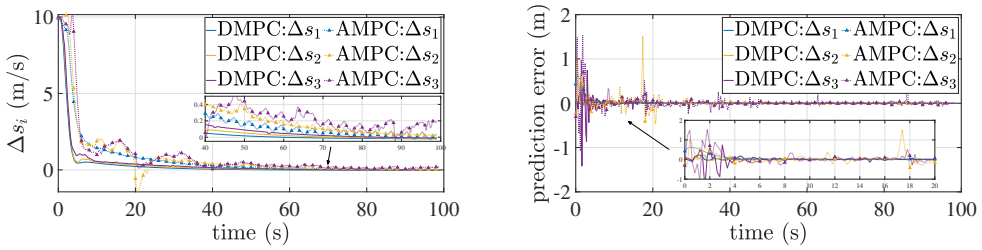

(a) (b)

Figure 6: Comparison of DMPC and AMPC: (a) smoothness; (b) modeling accuracy.

The controller of AMPC is yielded by solving the following OCP:

$$\min_{\hat{x}_i(\cdot|k),\hat{u}_i(\cdot|k)} J_i'(k) = \sum_{j=0}^{N-1} \|\hat{x}_i(j|k) - r\|_Q^2 + \|\hat{u}_i(j|k)\|_R^2 \tag{34a}$$

s.t. constraints (24d)-(24g), (29b) and

$$\hat{x}_i(j+1|k) = \hat{A}_{i,k}\hat{x}_i(j|k) + \hat{B}_{i,k}\hat{u}_i(j|k)) \tag{34b}$$

where $\hat{A}_{i,k}$ and $\hat{B}_{i,k}$ are adaptively updated by least-square regression based on $x_i([k-15:k])$ and $u_i([k-15:k-1])$. To guarantee PE conditions, we add a multi-frequency sinusoidal signal onto the optimal controller from AMPC. This approach can be seen as an extension of Luo et al. (2021).

To compare the performance, we apply AMPC in the same cruising case as above. The error of following distance controlled by AMPC are compared with our approach in Figure 6(a). We can find that our approach is prone to more smooth operations. The underlying reason is that the past trajectories must be PE due to the requirements from online system identification, which will causes non-smooth operations. However, our approach only requires PE for the data trajectories, which does not influence the actual operation.

Another advantage of our approach is higher modeling accuracy, as shown in Figure 6(b). It comes from the enough large database. However, in AMPC, the length of past trajectories cannot be excessive long, since: (1) VCTS needs to go through a long-time operation without AMPC; (2) Long trajectories might lead into overfitting.

4.2.4. Generalization Performance: Compared with Learning Control

As an effective model-free control approach for non-analytic systems, reinforcement learning (RL) could potentially address VCTS operation well. Thus, we employ the RL approach in and compare the performance with our approach.

5. Conclusion

Acknowledgment

This work was supported by the National Natural Science Foundation of China (52372310, 52172322, 52372309, U22A2046), the State Key Laboratory of Advanced Rail Autonomous Operation (RAO2023ZZ001), the Fundamental Research Funds for the Central Universities (2023JBZY013, 2022JBQY001) and Beijing Laboratory of Urban Rail Transit.

References

Aoun, J., Quaglietta, E., Goverde, R.M., 2023. Roadmap development for the deployment of virtual coupling in railway signalling. Technological Forecasting and Social Change 189, 122263–122263. URL: https://www.sciencedirect.com/science/article/pii/S0040162522007843, doi:https://doi.org/10.1016/j.techfore.2022.122263.

Berberich, J., Kohler, J., Muller, M.A., Allgower, F., 2021. Data-driven model predictive control with stability and robustness guarantees. IEEE transactions on automatic control 66, 1702–1717. URL: https://ieeexplore.ieee.org/document/9109670, doi:https://doi.org/10.1109/tac.2020.3000182.

Berberich, J., Köhler, J., Müller, M.A., Allgöwer, F., 2022a. Linear tracking mpc for nonlinear systems—part i: The model-based case. IEEE Transactions on Automatic Control 67, 4390–4405. URL: https://ieeexplore.ieee.org/document/9756294, doi:https://doi.org/10.1109/tac.2022.3166872.

Berberich, J., Köhler, J., Müller, M.A., Allgöwer, F., 2022b. Linear tracking mpc for nonlinear systems—part ii: The data-driven case. IEEE Transactions on Automatic Control 67, 4406–4421. URL: https://ieeexplore.ieee.org/document/9756053, doi:https://doi.org/10.1109/tac.2022.3166851.

Bian, Y., Du, C., Hu, M., Li, S.E., Liu, H., Li, C., 2022. Fuel economy optimization for platooning vehicle swarms via distributed economic model predictive control. IEEE Transactions on Automation Science and Engineering 19, 2711–2723. URL: https://ieeexplore.ieee.org/abstract/document/9627936, doi:https://doi.org/10.1109/tase.2021.3128920.

Bongard, J., Berberich, J., Köhler, J., Allgöwer, F., 2023. Robust stability analysis of a simple data-driven model predictive control approach. IEEE transactions on automatic control 68, 2625–2637. URL: https://ieeexplore.ieee.org/document/9744574, doi:https://doi.org/10.1109/tac.2022.3163110.

Chai, M., Wang, H., Tang, T., Chai, J., Liu, H., 2024. A relative operation-based separation model for safe distances of virtually coupled trains. IEEE transactions on intelligent vehicles 9, 2031–2045. URL: https://ieeexplore.ieee.org/abstract/document/10202588, doi:https://doi.org/10.1109/tiv.2023.3301009.

Felez, J., Vaquero-Serrano, M.A., 2023. Virtual coupling in railways: A comprehensive review. Machines 11, 521. URL: https://www.mdpi.com/2075-1702/11/5/521, doi:https://doi.org/10.3390/machines11050521.

Kohler, J., Allgower, F., 2019. Nonlinear reference tracking: An economic model predictive control perspective. IEEE Transactions on Automatic Control 64, 254–269. URL: https://ieeexplore.ieee.org/document/8278210, doi:https://doi.org/10.1109/tac.2018.2800789.

Liu, H., Luo, X., Tang, T., Zhang, Y., Chai, M., 2023. A hierarchical control approach for virtual coupling in metro trains. Computer-Aided Civil and Infrastructure Engineering URL: https://onlinelibrary.wiley.com/doi/10.1111/mice.13138, doi:https://doi.org/10.1111/mice.13138.

Luo, X., Gao, J., Zhang, Y., Han, X., Liu, H., 2023. A feedforward pid control approach for reference tracking of virtually coupled train set URL: https://ieeexplore.ieee.org/document/10422350, doi:https://doi.org/10.1109/itsc57777.2023.10422350.

Luo, X., Tang, T., Li, K., Liu, H., 2024a. Computation-efficient distributed mpc for dynamic coupling of virtually coupled train set. Control Engineering Practice 145, 105846–105846. URL: https://www.sciencedirect.com/science/article/pii/S0967066124000066, doi:https://doi.org/10.1016/j.conengprac.2024.105846.

Luo, X., Tang, T., Liu, H., Zhang, L., Li, K., 2021. An adaptive model predictive control system for virtual coupling in metros. Actuators 10, 178.

Luo, X., Tang, T., Wang, W., Ji, Y., Liu, H., 2024b. Distributed nonlinear model predictive control for virtually coupled train set with relative-braking distance. IEEE transactions on intelligent transportation systems (under review) .

Quaglietta, E., Wang, M., Goverde, R., 2020. A multi-state train-following model for the analysis of virtual coupling railway operations. Journal of Rail Transport Planning & Management 15, 100195.

Wang, J., Liu, H., Tang, T., Luo, X., Chai, M., 2022. A space-time interval based protection method for virtual coupling. 2022 China Automation Congress (CAC) URL: https://ieeexplore.ieee.org/document/10055304, doi:https://doi.org/10.1109/cac57257.2022.10055304.

Wu, Q., Ge, X., Han, Q.L., Liu, Y., 2023. Railway virtual coupling: A survey of emerging control techniques. IEEE Transactions on Intelligent Vehicles , 1–17URL: https://ieeexplore.ieee.org/abstract/document/10079173, doi:https://doi.org/10.1109/tiv.2023.3260851.

Xun, J., Li, Y., Liu, R., Li, Y., Liu, Y., 2022. A survey on control methods for virtual coupling in railway operation. IEEE Open Journal of Intelligent Transportation Systems 3, 838–855. URL: https://ieeexplore.ieee.org/document/9978693, doi:https://doi.org/10.1109/ojits.2022.3228077.

Zhao, Y., Ioannou, P., 2015. Positive train control with dynamic headway based on an active communication system. IEEE Transactions on Intelligent Transportation Systems 16, 3095–3103. doi:10.1109/TITS.2015.2435515.